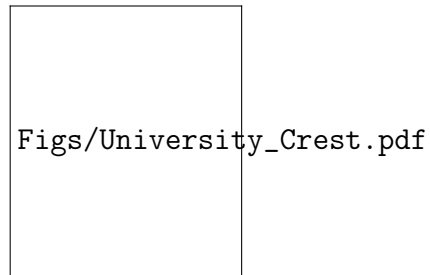


Geometry and shape inversion in *Choanoeca flexa*



Adam Konkol

Advisor: Dr. R. E. Gold-
stein

Department of Physics
University of Cambridge

This thesis is submitted for the degree of
Master of Philosophy

I would like to dedicate this thesis to my loving parents ...

ak2351: dedicate to people!

Declaration

I hereby declare that except where specific reference is made to the work of others, the contents of this dissertation are original and have not been submitted in whole or in part for consideration for any other degree or qualification in this, or any other university. This thesis is my own work and includes nothing which is the outcome of work done in collaboration except where specifically indicated in the text. This thesis contains fewer than 15,000 words including appendices, bibliography, footnotes, and tables.

Adam Konkol

July 2022

Acknowledgements

And I would like to acknowledge ...

ak2351: acknowledge people!

Abstract

The newly discovered multicellular choanoflagellate *Choanoeca flexa* forms a curved sheet that undergoes a functional, light-triggered inversion. This change in orientation that allows the organism to reversibly switch between efficient swimming and feeding shapes provides an opportunity to study biological exploitation of geometry in an evolutionarily basal context. I sought to model the mechanics that produce this apparent bistability and the dynamics of the active transformation between the two states.

In this work, I approach the modeling problem from complementary continuous and discrete mechanics perspectives. Since radial expansion and contraction at a given latitude require azimuthal stretching and shrinking, a one-dimensional filament model does not capture the energetic barriers encountered by the sheet during the transition. Using energy functional variation, I solve for the forces acting throughout the sheet and derive corresponding equilibrium shape equations. Both views establish that *C. flexa* inversion can be hindered in sufficiently large sheets by cell collars connecting adjacent cells stretching.

Comparisons between the discrete model for *C. flexa* mechanics and previously published experimental results support that collar stretching at the edges interferes in sheet inversion. Treating the organism as a crystal lattice defined by cells and cell-cell interactions, we recognise that the graph degree of cells plays a substantial role in overall sheet curvature and ability to invert.

My results suggest that the graph topology of the cell-cell interface network must accommodate inversion, particularly at the edge of the sheet. Future work should image *C. flexa* flipping and observe changes in connectivity that accompany the transition. My results link graph topology with a notion of surface curvature through established ideas in the theory of crystal structure.

Table of contents

List of figures	xiii
List of tables	xv
1 Introduction	1
1.1 Background	1
1.2 Choanoflagellates	1
1.3 <i>Choanoeca flexa</i>	2
1.4 Thesis overview	3
2 Continuous model	5
2.1 One-dimensional model	5
2.2 Surface approximation	8
2.2.1 H and collar connection angle	10
2.2.2 Problem statement	11
2.2.3 Connecting continuous surface with individual cell mechanics . . .	12
2.2.4 Writing the energy	15
2.2.5 Varying the energy	16
2.3 Energy variation	17
3 Discrete model	19
3.1 Discrete model	19
3.1.1 Sheet energy	19
3.1.2 Graph topology	20
3.2 Everything before written	20
3.3 Discrete surface model	20
3.3.1 How to define the surface	20
3.3.2 Surface formed by collar boundaries	21

3.3.3	Surface formed by cell bodies	23
3.4	Including both cells and collar boundaries	23
3.4.1	Initial sheet	23
3.4.2	Bending energies	27
3.4.3	Minimising sheet energy	30
3.4.4	Numerical optimisation routine	30
3.4.5	Topology	33
3.4.6	Larger cell sheets	33
3.5	Varying the energy	38
4	Discussion	39
4.1	section	39
	References	41

List of figures

2.1	Solving the boundary value problem in equation 2.6	7
2.2	Time evolution of a one-dimensional filament which switches prescribed curvature sign instantaneously. Time and length are given in dimensionless units defined by the length L , bending modulus A , and drag coefficient ζ . The time unlabeled time intervals continue sequentially in intervals of $\Delta t = 3 \times 10^{-4}$	9
2.3	Geometry for relating collar boundary angle ψ to curvature H	10
2.4	Geometry of a single cell and collar with a continuous surface approximating the interactions between collars.	13
2.5	Maximum cell-side curvature is given by inequalities 2.13, 2.14 to have radius ℓ . This corresponds to every (point) cell bumping into each other. . .	14
3.1	Two views of the physical dual graphs used in describing <i>C. flexa</i>	21
3.2	Voronoi tessellation of initial cell placement. Cell bodies shown in blue points, collar boundaries shown in black lines with collar boundary end points shown in orange. Notably, the regions corresponding to boundary cells extend out to infinity. We need to add all boundary collar vertices along the infinite dashed lines.	24
3.3	Initial layout for the flexa sheet. Cell bodies are shown in large purple points and collar boundary vertices are shown in small yellow points. Black edges connect cells to collar boundary vertices, and orange edges show cell-cell neighbor relations (though these orange edges are not physically present). The physical interactions are mediated through the black edges.	26
3.4	Figure in the same style of Figure 3.3 showing the cell sheet projected onto the xy -plane after minimising energy.	31

3.5	Cell sheet geometry from the hexagonal lattice in Figure 3.3 and parameters (3.5a) $\phi_0 = 0.99\phi_{\text{init}}$, $\phi_0 = 1.03\psi_{\text{init}}$, $\ell_0 = \ell_{\text{init}} = 1.52$, (3.5b) $\phi_0 = 0.9\phi_{\text{init}}$, $\psi_0 = 1.15\psi_{\text{init}}$, $\ell_0 = \ell_{\text{init}} = 1.52$	32
3.6	Cell sheet geometry with noise added to the initial lattice. The graph topology is affected at the sheet boundary (subfigure 3.6a) from the Voronoi tessellation. This minor change has substantial effects on the sheet geometry (subfigures 3.6b, 3.6c).	34
3.7	Cell sheet geometry with a node of degree 7. The graph topology is affected in the sheet interior (subfigure 3.7a). This minor change has substantial effects on the sheet geometry (subfigures 3.7b, 3.7c).	35
3.8	Cell sheet geometry with a node of degree 7. The graph topology is affected in the sheet interior (subfigure 3.8a). This minor change has substantial effects on the sheet geometry (subfigures 3.8b, 3.8c).	36
3.9	Cell sheet geometry with a node of degree 7. The graph topology is affected in the sheet interior (subfigure 3.9a). This minor change has substantial effects on the sheet geometry (subfigures 3.9b, 3.9c).	37

List of tables

Chapter 1

Introduction

1.1 Background

Thesis statement: studying evolutionarily basal organisms lets us study the simple ways that nature exploits geometry in living systems without higher order functional complications.

Discuss evolutionary origins of multicellularity and some basic examples like *Volvox*. What drives organisms to become multicellular?

The organisms in the *Volvox* genus are well studied for being a primitive example of multicellularity and a shining beacon of functional geometric changes. These organisms attach their cells to one another using an extra-cellular matrix, as *S. rosetta* does as well (discussed later).

We are interested in multicellularity at an evolutionarily basal level to understand the basic reasons that life evolved to form multicellular organisms. Sponges are as basal as multicellular animal life goes

ak2351: Discuss why and reference a review about sponges evolutionary simplicity. Carr et al. [4] could be a good ref to give here regarding choanoflagellates

While we are interested in sponges since they are members of the animal kingdom, choanoflagellates are often considered to be evolutionarily and morphologically comparable.

1.2 Choanoflagellates

ak2351: Discuss Carr et al. [4] about molecular phylogeny of choanoflagellates

Mah et al. [9] offers the first comprehensive comparison between sponge choanocyte and choanoflagellate morphology. Sponge collars are fairly cylindrical while choanoflagellate collars are more cone-like. Choanoflagellates have glycocalyx, but seemingly around the cell body [8]. Notably the collars in choanoflagellates are always microvillar and always present, while in sponges they emerge as a consequence of cell differentiation

ak2351: cite this!

.
ak2351: this is an old connection, though. James-Clark (1868) first describes the similarities. Tuzet (1963) finds that they have a common ancestor but not that sponges evolved from choanoflagellates. see references in first paragraph of ?].

Choanoflagellates are increasingly studied as a model for understanding how multicellular animal life emerged. Fairclough et al. [5] shows that the transition from single cell to multicellular colony in *Salpingoeca rosetta* occurs by cell division, with cells remaining attached to each other.

S. rosetta has an extracellular matrix [7]. Larson et al. [7] finds that the extracellular matrix constrains cells to grow and divide to a given colony shape. This paper also finds that *S. rosetta* does not have distinct cell lineages or a developmental plan.

Kirkegaard and Goldstein [6] finds that collared choanoflagellates drive the most flow through their collars by swimming fastest, which occurs in the unicellular state [10]. This makes it unclear that forming rosette colonies is for the sake of improved feeding. The authors point to evidence that *S. rosetta* is induced to form rosette colonies by bacterial cues to suggest that the reasons for the development of multicellularity may be more subtle than previously expected [1].

1.3 *Choanoeca flexa*

Brunet et al. [3] describe a newly discovered choanoflagellate, *Choanoeca flexa*, which lives and feeds in aquatic environments. Here, I describe the relevant properties and characteristics of these cells and their colonies for modeling its structure and behavior. All descriptions proceed from Brunet et al. [3] and private communications with the authors.

Another sheet forming-choanoflagellate was described in ?], *Proterospongia choano-juncta*.

Shape inversion: swimming/feeding, light triggered, dynamics of process Connected by collars, (presumed) active transformation via contractile ring. This differs from choanoflag-

ellates like *S. rosetta* which use ECM [7]. Likely stiff actin collars with some intrinsic curvature and potentially different stiffness between the two states.

If other choanoflagellates are any indication, we know in *S. rosetta* that cell division is asynchronous [5]. If *C. flexa* forms colonies by a similar mechanism, then we might not expect regularity in its structure.

ak2351: this need not be true! What would asynchronous cell division indicate about structure?

We are interested in this species because we hope we can use its colonies' geometries as a model for sponge choanocyte chambers and more broadly to understand how life most simply exploits shape at a multicellular level. It is quite difficult to experimentally model flows in the choanocyte chamber [?], and published results on choanocyte flow have only been computational. Understanding the geometry of *C. flexa* can contribute to understanding the flows that a colony can drive, which will contribute to the growing body of knowledge on flows driven by several pumps positioned along a surface [2].

1.4 Thesis overview

The thesis will be structured in this way.

Chapter 2

1

Continuous model

2

Sheets of *C. flexa*, despite being discretely made up of individual cells, appear to take on curvature when looked at as a whole. In an effort to avoid the complexity of tracking a cell-cell connection network, I approximated sheets of *C. flexa* with continuous surfaces.

3

4

5

I begin by developing a one-dimensional filament model with inversion dynamics, which demonstrates that azimuthal stretching is key to understanding the flipping process observed in Brunet et al. [3]. I proceed to describe a method for approximating sheets of *C. flexa* with two-dimensional surfaces and relate the collar-opening angle ϕ and collar-collar contact angle ψ to surface curvature. I write an expression for the sheet energy and vary it to derive a shape equation.

6

7

8

9

10

11

2.1 One-dimensional model

12

We are interested in the problem of *Choaneca flexa* inversion. For intuition, suppose we have a one dimensional filament with position $\vec{r}(s)$ parameterised by arclength s . If the filament has prescribed curvature κ_0 , then the bending energy functional \mathcal{E} is given by

13

14

15

$$\mathcal{E}[\vec{r}(s)] = \frac{1}{2}A \int (\kappa - \kappa_0)^2 ds,$$

16

17

where the curvature κ is deduced from $\vec{r}(s)$ and A is the bending modulus. If the filament is short relative to the characteristic bending length scale, we express the problem in the Mange representation by writing $\vec{r}(s) = (x, h(x))$ for a height function $h(x)$. The resulting energy is written in terms of the prescribed (signed) curvature H_0 ,

$$\varepsilon[\vec{h}(x)] = \frac{1}{2}A \int_0^L (h_{xx} - H_0)^2 dx. \quad (2.1)$$

We postulate that the filament experiences isotropic drag with coefficient ζ in a viscous medium, with the dynamics are described by a functional derivative of the energy:

$$\begin{aligned} \zeta \vec{r}_t &= -\frac{\delta \varepsilon}{\delta \vec{r}} \\ \zeta h_t &= -\frac{\delta \varepsilon}{\delta h}. \end{aligned} \quad (2.2)$$

Taking the functional derivative of equation 2.1, we find the energy change

$$\delta \varepsilon = A(h_{xx} - H_0)\delta h_x|_0^L - Ah_{3x}\delta h|_0^L + A \int h_{4x}\delta h ds \quad (2.3)$$

in terms of the boundary conditions of h .

$$(2.4)$$

If we take free-end boundary conditions $h_{xx}(0, L) = 0 = h_{3x}(0, L)$, the boundary terms in equation 2.3 vanish and we are left with the equation of motion

$$\zeta h_t = -Ah_{4x} \quad (2.5)$$

We nondimensionalise equation 2.5 by re-expressing x as x/L and t as $t/(\frac{\zeta L^4}{A})$ (the labels x, t, h, H_0 are left unchanged for readability) to derive $h_t = -h_{4x}$ with boundary conditions $h_{xx}(0, 1) = 0 = h_{3x}(0, L)$. It is clear that the ground state of equation 2.1 is given by a quadratic height function with quadratic term $\frac{1}{2}H_0x^2$. Let $h_*(x) = -\frac{1}{2}H_0(x - \frac{1}{2})^2 + \frac{1}{8}H_0$ be

2.1 One-dimensional model

7

one such ground state, and suppose $h(x, 0) = -h_*(x)$. Note that the filament in $h(x, 0)$ is not in the ground state since the curvature is given by H_0 .

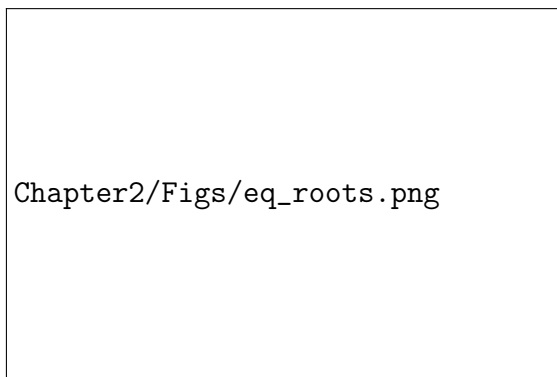
The dynamics of the displacement $g(x, t) = h(x, t) - h_*(x)$ is given by $g_t = g_{4x}$. If $g(x, t) = e^{-\sigma t} f(x)$ for some $f(x)$ and eigenvalue σ , we obtain the ordinary boundary value problem

$$\frac{d^4 f}{dx^4} = \sigma f \quad \begin{cases} f''(0, 1) = 0 \\ f'''(0, 1) = 0. \end{cases} \quad (2.6)$$

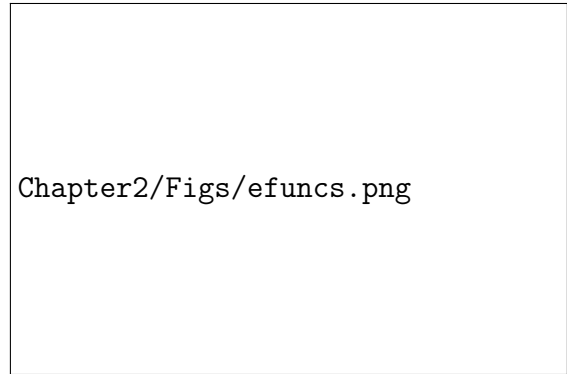
It is clear that the general solution of f is $A \sin kx + B \cos kx + D \sinh kx + E \cosh kx$. As in BPDFD 4.2.3, the derivatives $f''(0) = f'''(0) = 0$ gives $A = D, B = E$. Moreover, the eigenvalues $\sigma = k^4$ are given by the sequence of solutions k_n to

$$\cos k - \frac{1}{\cosh k} = 0. \quad (2.7)$$

Equation 2.7 is plotted in Figure 2.1a along with the positions of the solutions k_n as solved numerically. The solution $k_0 = 0$ is omitted because it contributes a constant term to $h(x, t)$ that does not evolve in time. The eigenfunctions $w_n(x)$ with eigenvalues k_n^4 are normalized on the interval $[0, 1]$ numerically, and the ratio A/B is given by $(\sinh k - \sin(k))/(\cosh k - \cos k)$. The first five eigenfunctions are shown in Figure 2.1b.



(a) Equation 2.7 and its solutions.



(b) The first five eigenfunctions f_n of boundary value problem 2.6.

Fig. 2.1 Solving the boundary value problem in equation 2.6

Letting $f(x) = \sum_{n=1}^{\infty} a_n f_n(x)$, we get that $a_n = \int_0^1 g(x, 0) f_n(x) dx$, and the complete dynamics of the height function are given by

$$h(x, t) = h_*(x) + g(x) = h_*(x) + \sum_{n=1}^{\infty} a_n e^{k_n^4 t} f_n(x). \quad (2.8)$$

In practice, only the solutions k_n to equation 2.7 shown in Figure 2.1a are used, since the approximation to $h(x, 0)$ is close and higher k_n result in precision errors when calculating $\cosh kx$ and $\sinh kx$.

For the initial conditions given previously, the time evolution of $h(x, t)$ is shown in Figure 2.2. We can make a few observations:

- The system evolves extremely quickly in non-dimensional time. This is because each mode's evolution is given by rate k_n^4 , which grows rapidly and makes higher order terms negligible almost immediately. Maybe it is worth asking what the values of the bending modulus and drag coefficient are to see if the timescale $\zeta L^4/A$ is very large to compensate.
- The time evolution slows at larger t . This makes sense as the change in energy $\delta\mathcal{E}$ becomes smaller in magnitude when the curvature $h_{xx}(x, t)$ becomes closer to that of $h_*(x, t)$.
- We see some “rolling inward” of the change in curvature from the outer edge, most clearly at $t = 9 \times 10^{-4}$. However, it does not seem as pronounced as in *C. flexa* inversion, at least not to me. When the organism inverts, it seems to have a wave of flipping that moves from the edge towards the center. Perhaps this is because the *C. flexa* collars are stiff such that they resist compression or stretching in the sheet. Our representation used here does not penalize the filament compressing, which it clearly does as its arclength decreases substantially during the transition.

2.2 Surface approximation

The simplified dynamics that we get from the Mange representation lack energetic costs from the compression and extension that come with deforming a two dimensional surface. The logical step to include these energies is to model the flexa sheet a surface of revolution based on a curve $\mathbf{r}(\rho, \theta) = (\rho \cos \theta, \rho \sin \theta, z(\rho))$ with cylindrical coordinates ρ, θ and height function z . In doing so, we could take the elastohydrodynamic equation of motion written in terms of curvature H and K and express it as purely as a function of z .

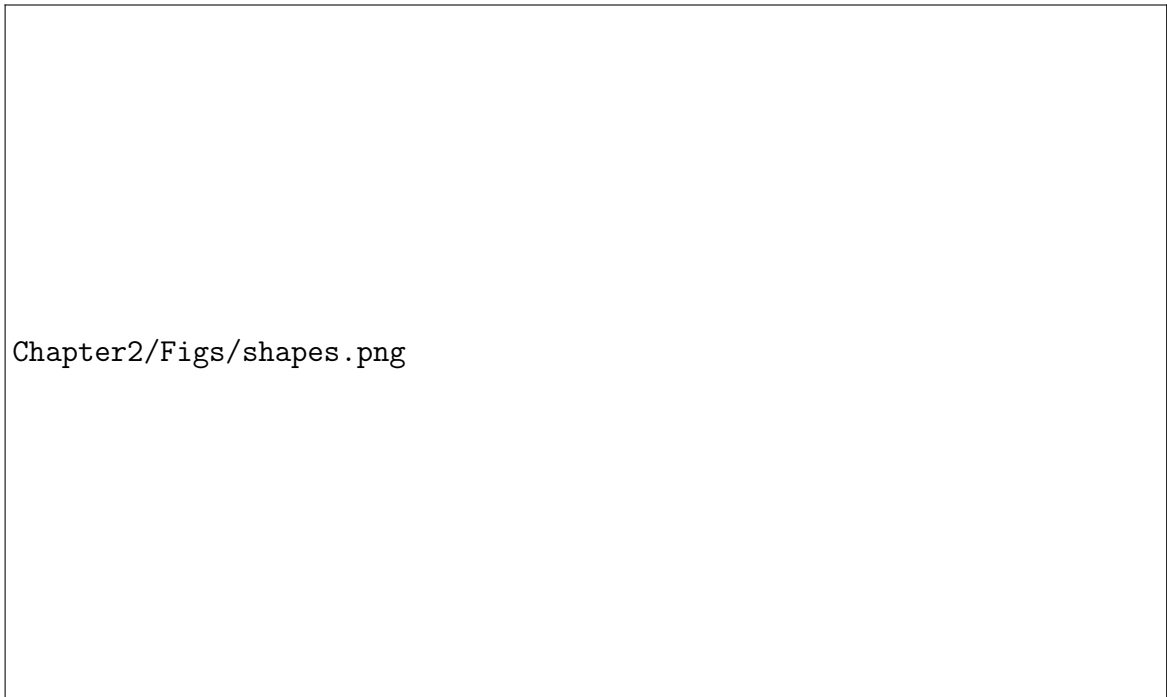


Fig. 2.2 Time evolution of a one-dimensional filament which switches prescribed curvature sign instantaneously. Time and length are given in dimensionless units defined by the length L , bending modulus A , and drag coefficient ζ . The time unlabeled time intervals continue sequentially in intervals of $\Delta t = 3 \times 10^{-4}$.

We will proceed by writing the equations of motion generally for a surface and reducing it to a surface of revolution.

2.2.1 H and collar connection angle

Before getting into the continuous sheet problem, it is worth describing the two degrees of freedom that our collar connections afford. The collar makes an angle ϕ between the vector pointing directly out of the cell and the vector between the cell and its collar boundary with the next cell. Additionally, there is an angle between the collars of two adjacent cells ψ . The latter results in the sheet's curvature, so we want to relate it to mean curvature H or preferred curvature H_0 .

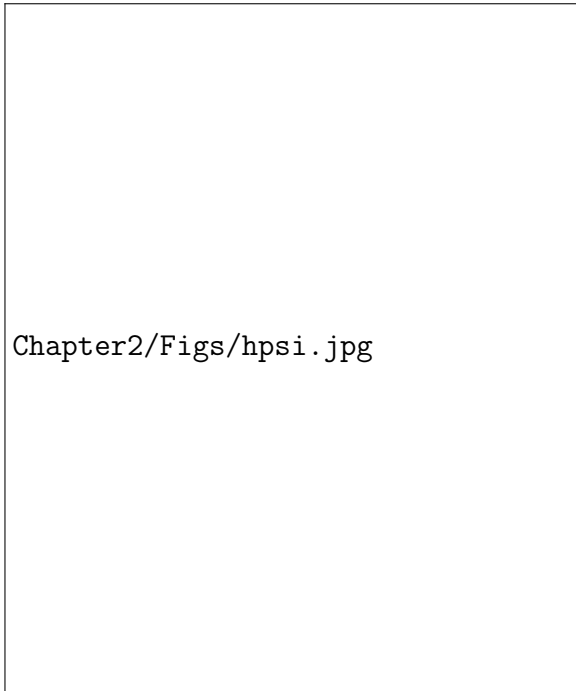


Fig. 2.3 Geometry for relating collar boundary angle ψ to curvature H .

Consider two neighboring cells with collar boundaries a , b , and c , as shown in Figure 2.3. We might imagine defining a radius of curvature by the circle that passes through the three collar boundaries. If we set $\mathbf{x}_a = 2\ell \sin \phi_0 (-1, 0)$, $\mathbf{x}_b = (0, 0)$, and $\mathbf{x}_c = 2\ell \sin \phi_0 (\sin(\psi_0 - \phi_0), \cos(\psi_0 - \phi_0))$, we can solve for the circle coordinates

$$(x_o, y_o) = \ell \sin \phi_0 \left(-1, \frac{1 + \cos 2(\psi_0 - \phi_0)}{\sin 2(\psi_0 - \phi_0)} \right)$$

to get the inverse radius of curvature

$$H_0 = \frac{1}{\sqrt{x_0^2 + y_0^2}} = \frac{\sin(\psi_0 - \phi_0)}{\ell \sin \phi_0}. \quad (2.9)$$

This has a nice, simple interpretation in that if $\psi_0 > \phi_0$, $H_0 > 0$ (as drawn in Figure 2.3). On the other hand, $\psi_0 < \phi_0$ implies $H_0 < 0$, or the sheet is concave on the cell body side.

Alternatively, we solve for ψ_0 as a function of H_0 ,

$$\psi_0 = \phi_0 + \arcsin(H_0 \ell \sin \phi_0). \quad (2.10)$$

As we find later in equation 2.15, the curvature of the sheet in any given direction is greater than or equal to $-1/\ell$ (cell bodies and collars cannot go through each other). This lower bound corresponds in 2.10 to $\psi_0 = 0$, which we expect when cells are pressing tightly against each other (Figure 2.5).

2.2.2 Problem statement

Powers [11] (Section IV.B) shows that for an energy density \mathcal{E} written in terms of the first and second fundamental forms $g_{\alpha\beta}$ and $K_{\alpha\beta}$, we can write an expression for the stress tensor \mathbf{F}^α

$$\mathbf{F}^\alpha = \left(T^{\alpha\beta} + \mathcal{E}^{\alpha\beta} K_\gamma^\beta \right) \mathbf{t}_\beta - (\nabla_\beta \mathcal{E}^{\alpha\beta}) \hat{\mathbf{n}}. \quad (2.11)$$

Here, $K_\gamma^\beta = K_{\gamma\delta} g^{\delta\beta}$, $\mathbf{t}_\beta = \partial_\beta \mathbf{r}$, and

$$T^{\alpha\beta} = g^{\alpha\beta} \mathcal{E} + 2 \frac{\partial \mathcal{E}}{\partial g_{\alpha\beta}} = \frac{2}{\sqrt{g}} \frac{\partial}{\partial g_{\alpha\beta}} (\sqrt{g} \mathcal{E})$$

$$\mathcal{E}^{\alpha\beta} = \frac{\partial \mathcal{E}}{\partial K_{\alpha\beta}}$$

with $g = \det g_{\alpha\beta}$.

Since the force \mathbf{f} acting on a surface point is given by the covariant divergence of the stress $\nabla_\alpha \mathbf{F}^\alpha$, our problem is effectively solved once we decide on an appropriate energy

density. Brunet et al. [3] showed that the angle formed by the *C. flexa* collars changes when individual cells are triggered for inversion. We might reasonably suggest preferred sheet curvature is prescribed by changing the preferred angle of the collar ϕ_0 and imposing an energetic cost based on the amount that the collar angle $\phi(\theta)$ differs around the collar in θ : $\mathcal{E} \sim \int (\phi(\theta) - \phi_0)^2 d\theta$.

2.2.3 Connecting continuous surface with individual cell mechanics

For any point on a smooth surface, we could find an orthonormal basis of eigenvectors $\mathbf{e}_1, \mathbf{e}_2$ in the tangent space that diagonalises K_μ^ν . In terms of a vector $\Delta \xi$ written in this basis, we have that the change in height with respect to the tangent plane and its normal Δh is given by $K_{\mu\nu} \Delta \xi^\mu \Delta \xi^\nu$.

Let's consider a cell with collar angle $\phi(\theta)$, where θ measures the location on the collar. If the cell has an optimal collar angle ϕ_0 and corresponding optimal curvature $K_{0\mu\nu}$, then the height of the collar will be $K_{0\mu\nu} \Delta \xi_0^\mu \Delta \xi_0^\nu$. The distance from the centerline of the cell (the norm of $\Delta \xi_0$) is determined by ϕ_0 . The geometry is shown in Figure 2.4.

If the cell has collar angle ϕ in direction θ , we know the collar distance as $\Delta \xi = \ell(\cos \phi, \sin \phi)$. For a fixed collar length ℓ , we know the difference in height between the ground state and deformed state is $\ell(\cos \phi - \cos \phi_0)$. We can then relate the collar angle and sheet curvature by equating

$$K_{\mu\nu} \Delta \xi^\mu \Delta \xi^\nu - K_{0\mu\nu} \Delta \xi_0^\mu \Delta \xi_0^\nu = \ell(\cos \phi - \cos \phi_0). \quad (2.12)$$

The radius out from the center for the ground state is $\ell \sin \phi_0$ while for the deformed state it is $\ell \sin \phi$, so for $K_{011} = K_{022} = H_0$, we get

$$\begin{aligned} K_{\mu\nu} \ell^2 \sin^2 \phi (\cos \theta, \sin \theta)^{\mu,\nu} - H_0 \ell^2 \sin^2 \phi_0 &= \ell(\cos \phi - \cos \phi_0) \\ H_\theta \ell^2 \sin^2 \phi - H_0 \ell^2 \sin^2 \phi_0 &= \ell(\cos \phi - \cos \phi_0) \end{aligned}$$

where $H_\theta = K_{11} \cos^2 \theta + K_{22} \sin^2 \theta + 2K_{12} \sin \theta \cos \theta$ is the curvature of a line on the surface in direction θ . We can cancel a factor of ℓ , redefine units of length in terms of ℓ (such that H_θ is the ratio of ℓ with the radius of curvature in direction θ), and express $\sin^2 \phi$ in terms of $\cos \phi$ to get

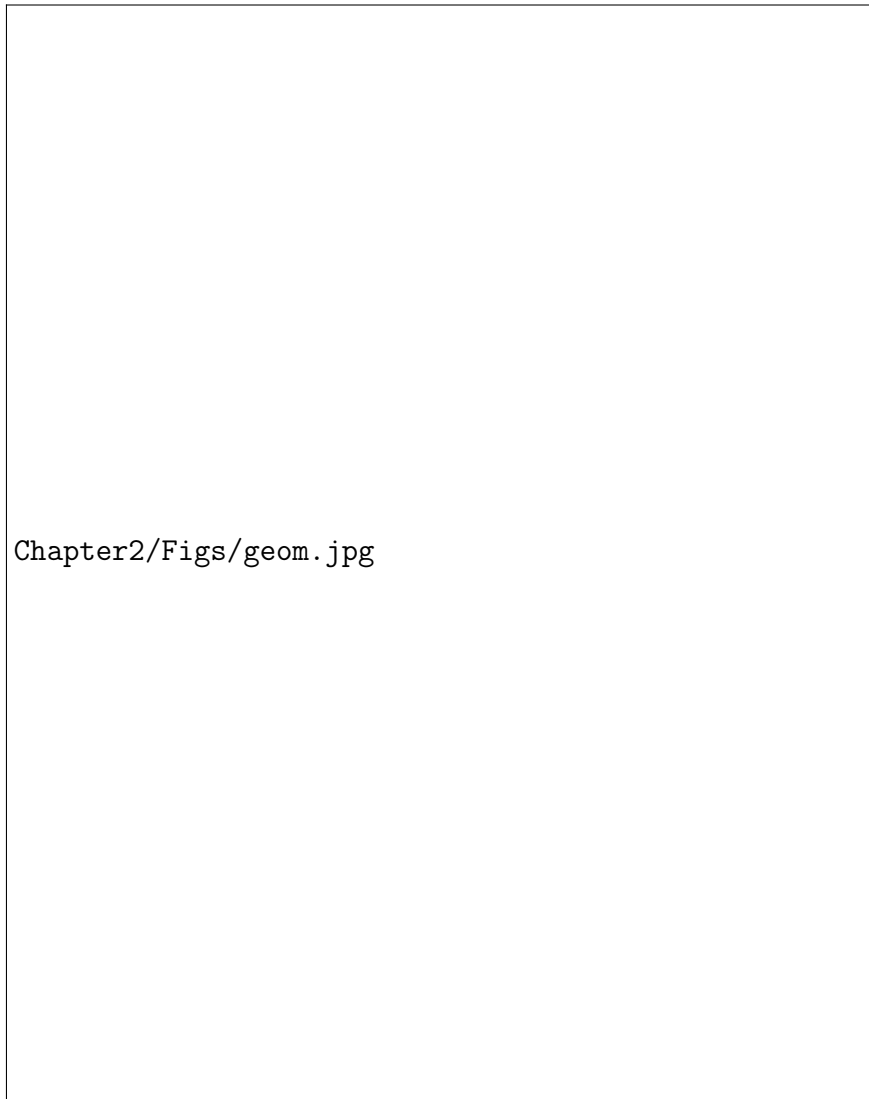


Fig. 2.4 Geometry of a single cell and collar with a continuous surface approximating the interactions between collars.

$$0 = H_\theta \cos^2 \phi + \cos \phi + (H_0 \sin^2 \phi_0 - \cos \phi_0 - H_\theta)$$

$$\cos \phi = \frac{-1 \pm \sqrt{1 + 4H_\theta(H_\theta + \cos \phi_0 - H_0 \sin^2 \phi_0)}}{2H_\theta}.$$

If we take the collars to always have angle $0 \leq \phi \leq \pi/2$, we can constrain $0 \leq \cos \phi \leq 1$ to find the two inequalities

$$H_\theta \geq H_0 \sin^2 \phi_0 - \cos \phi_0 \quad (2.13)$$

$$1 \geq \cos \phi_0 - H_0 \sin^2 \phi_0. \quad (2.14)$$

The second inequality can be simplified to $H_0 \geq -(1 + \cos \phi_0)^{-1}$. Combining the two inequalities yields

$$H_\theta \geq -1. \quad (2.15)$$

Re-expressed with units, this means that $H_\theta \geq -1/\ell$, or that the radius of curvature can never be smaller than ℓ on the cells' side. In other words, the cells can't push through each other! (Figure 2.5)



Fig. 2.5 Maximum cell-side curvature is given by inequalities 2.13, 2.14 to have radius ℓ . This corresponds to every (point) cell bumping into each other.

2.2.4 Writing the energy

We want to write equation 2.12 in terms of $\phi - \phi_0$ to write down the energy. We can use a trigonometric identity to write

$$H_\theta \sin^2 \phi - H_0 \sin^2 \phi_0 = -2 \sin \frac{\phi - \phi_0}{2} \sin \frac{\phi + \phi_0}{2}. \quad (2.16)$$

If $\phi - \phi_0$ is small in magnitude, then

$$\begin{aligned} \sin \frac{\phi - \phi_0}{2} &\approx \frac{\phi - \phi_0}{2} \\ \sin \frac{\phi + \phi_0}{2} &= \sin \left(\phi_0 + \frac{\phi - \phi_0}{2} \right) \approx \sin \phi_0 + \frac{\phi - \phi_0}{2} \cos \phi_0 \\ \sin^2 \phi &= \sin^2 (\phi_0 + (\phi - \phi_0)) \approx \sin^2 \phi_0 + (\phi - \phi_0) \sin 2\phi_0. \end{aligned}$$

Using these approximations we rewrite equation 2.16 to first order in $\phi - \phi_0$ as

$$(H_\theta - H_0) \sin^2 \phi_0 + H_\theta (\phi - \phi_0) \sin 2\phi_0 = -(\phi - \phi_0) \sin \phi_0$$

$$(H_\theta - H_0) \sin^2 \phi_0 = -(\phi - \phi_0) (H_\theta \sin 2\phi_0 + \sin \phi_0)$$

$$\frac{(H_\theta - H_0)^2 \sin^4 \phi_0}{(H_\theta + \sin \phi_0 / \sin 2\phi_0)^2 \sin^2 2\phi_0} = (\phi - \phi_0)^2.$$

We want to integrate this function in θ , so let $K_{11} = a$, $K_{22} = b$, $K_{12} = c$, $-H_0 = d$ and $\sin \phi_0 / \sin 2\phi_0 = e$ for simplicity when we write

$$\begin{aligned}
& \int_{-\pi}^{\pi} (\phi - \phi_0)^2 d\theta = \int_{-\pi}^{\pi} \frac{(a \cos^2 \theta + b \sin^2 \theta + 2c \sin \theta \cos \theta + d)^2}{(a \cos^2 \theta + b \sin^2 \theta + 2c \sin \theta \cos \theta + e)^2} d\theta \\
& = \left\{ -\sin 2\theta \left[a^2(-4bc\theta - 4ce\theta + d^2 - 2de + e^2) + a(4b^2c\theta - 2b(d-e)^2 + 4c\theta(c^2 - e^2)) \right. \right. \\
& \quad \left. \left. + b^2(4ce\theta + d^2 - 2de + e^2) + 4bc\theta(e^2 - c^2) + 4c^2(d-e)^2 \right] \right. \\
& \quad \left. + 2(a+b+2e) \left[c^2\theta(b-a) + \theta(a-b)(a+e)(b+e) - c(d-e)^2 \right] \right. \\
& \quad \left. + 2\theta(a-b)^2 \cos(2\theta)(a(b+e) + e(b+e) - c^2) \right\} \\
& \quad / 2 \left[(a-b)(a(b+e) + e(b+e) - c^2)((a-b) \cos(2\theta) + a+b+2c \sin(2\theta) + 2e) \right] \\
& \quad (e-d)(a(4b+d+3e) + bd + 3be - 4c^2 + 2de + 2e^2) \tan^{-1} \left(\frac{-(b+e) \tan \theta - c}{\sqrt{a(b+e) + e(b+e) - c^2}} \right) \\
& \quad + \frac{2(a(b+e) + e(b+e) - c^2)^{3/2}}{2(a(b+e) + e(b+e) - c^2)^{3/2}}
\end{aligned}$$

evaluated at $\theta = -\pi, \pi$. Evaluating this expression is surprisingly straightforward, and gives the result

$$\int_{-\pi}^{\pi} (\phi - \phi_0)^2 d\theta = \text{const.} + \text{const.} \frac{4K + 2(d+3e)H + 2de + e^2}{(K + 2H + e^2)^{3/2}}.$$

Varying this expression will be more difficult than the typical membrane energy defined only in terms of curvature $(H - H_0)^2 + K$ since the Gaussian curvature term is not alone. This means that we cannot use the Gauss Bonnet theorem $\int_S K dA = 2\pi n + \oint_{\partial S} K ds$ to simply write it as a boundary term. Nevertheless, provided that we can vary K on the surface, the shape equation that results shouldn't be very difficult to derive.

2.2.5 Varying the energy

Following subsection 2.2.2, we just need to express our energy in terms of $K_{\mu\nu}$ and $g_{\mu\nu}$ to derive a force from it. We of course have that $H = (1/2)(K_{\mu\nu}g^{\mu\nu})$, which is easily differentiated with respect to $K_{\mu\nu}$ and $g_{\mu\nu}$. We can differentiate K by re-expressing it with the identity $K^{\alpha\beta}K_{\alpha\beta} = 4H^2 - 2K$.¹ Then we have $K = (g^{\alpha\beta}K_{\alpha\beta})^2 - K_{\mu\nu}K_{\alpha\beta}g^{\mu\alpha}g^{\nu\beta}$.

¹This comes from $4H^2 - 2K = (K_1^1 + K_2^2)^2 - 2(K_1^1K_2^2 - 2K_2^1) = (K_1^1)^2 + 2K_2^1K_2^1 + (K_2^2)^2 = K_\beta^\alpha K_\alpha^\beta = K^{\alpha\beta}K_{\alpha\beta}$.

2.3 Energy variation

Chapter 3

1

Discrete model

2

3.1 Discrete model

3

Why treat this as a discrete problem?

4

- More faithful treating as a discrete system. Allows/involves considerable simplification for collars (both a positive and negative)
- More tractable maths
- Computationally easier

5

6

7

8

3.1.1 Sheet energy

9

Defining a cell normal vector

10

Heuristic ways we might define it:

11

- Sum of vectors cell to collar. The issue is that this causes substantial boundary energy changes in ϕ
- plane approximation to collar: the issue is that cell position doesn't affect this at all, so we have to assume that the springs + normal approximation roughly produce a fair approximation

12

13

14

15

16

Or we could do it in full generality

17

Boundary effects

18

Why boundary collar nodes matter

19

Solving sheet shape

Numerical optimisation: sensitivity issues and initial conditions

Derive the gradient

Describe how to compute the gradient in an efficient way

3.1.2 Graph topology

For hexagonal lattice start, we

Call back to section 2.1

3.2 Everything before written

3.3 Discrete surface model

3.3.1 How to define the surface

We need to determine what parts of our physical problem we will keep track of, and how we will use them to define an energy. There are two natural, physical planar graphs to look at. We could either form the graph with cell bodies forming vertices and edges defined by cells whose collars make contact with each other. Alternatively, vertices could be represented by places where two cells' collars lose contact with each other, and edges could be along the line where those collars contact.

Since these graphs are planar (albeit not necessarily lying along a physical plane), we have a well-defined notion of a graph dual, where each face in one graph corresponds to a vertex in the other. What we find is that the two graphs described above are dual to each other (Figure 3.1a). One graph specifies the topology of the other, but we are considering these as spatial graphs to use their geometries so our problem is not so simple. Knowing the positions of all vertices and knowing the edges of one graph does not give complete information about the other.

Since each cell is identical, we might imagine that the distances between two cells and their mutual boundary is equal. In a loose sense, then, their interactions form a Voronoi tessellation on the surface of collar interactions (with respect to the metric on that surface). We can then take the dual to know that the graph of cell bodies is triangulated, as the dual of a Voronoi tessellation is a Delaunay triangulation (Figure 3.1b).

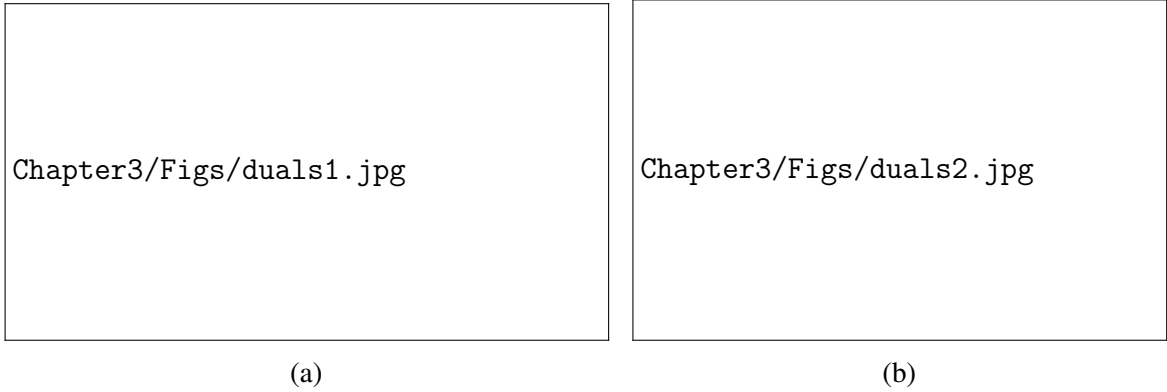


Fig. 3.1 Two views of the physical dual graphs used in describing *C. flexa*.

3.3.2 Surface formed by collar boundaries

Stretching

The physical interactions happen at the collar boundaries, so it makes sense to define energy based on the graph that quantifies them. If two cells have a collar boundary described by $\mathbf{r}_a t + (1-t)\mathbf{r}_b$ with $0 \leq t \leq 1$ and the energy is defined by continuously many springs from the boundary to a projected cell point \mathbf{r}_Δ , then the energy \mathcal{E}_{ab} of that boundary is

$$\mathcal{E}_{ab} = \int_0^1 [(\mathbf{r}_a t + (1-t)\mathbf{r}_b) - \mathbf{r}_\Delta]^2 dt = \frac{1}{3}(\mathbf{r}_a + \mathbf{r}_b)^2 - \frac{1}{3}\mathbf{r}_a \cdot \mathbf{r}_b - \mathbf{r}_\Delta \cdot (\mathbf{r}_a + \mathbf{r}_b) + \mathbf{r}_\Delta^2. \quad (3.1)$$

The energy corresponding to a cell consists of the line energies of all the collar interfaces. We find the position \mathbf{r}_Δ by setting the gradient of equation 3.1 with respect to \mathbf{r}_Δ to zero for all lines ab . If b indexes the vertices that cell Δ has, then

$$0 = \frac{d\mathcal{E}}{d\mathbf{r}_\Delta} = - \sum_{b \in \Delta} \mathbf{r}_b + 2n\mathbf{r}_\Delta$$

$$\mathbf{r}_\Delta = \frac{1}{n} \sum_{b \in \Delta} \mathbf{r}_b.$$

The force on vertex a is then given by the gradient of the whole sheet energy $\mathcal{E}_{\text{sheet}}$, which is the sum of the energies \mathcal{E}_Δ corresponding to each cell Δ .

$$\frac{d\mathcal{E}_{\text{sheet}}}{d\mathbf{r}_a} = \frac{d}{d\mathbf{r}_a} \sum_{\Delta} \mathcal{E}_{\Delta} = \sum_{\Delta: a \in \Delta} \frac{d\mathcal{E}_{\Delta}}{d\mathbf{r}_a} = \sum_{\Delta: a \in \Delta} \frac{d}{d\mathbf{r}_a} \sum_{b \in \Delta} (\mathbf{r}_b - \mathbf{r}_{\Delta})^2.$$

Since \mathbf{r}_{Δ} depends on \mathbf{r}_a itself, we write

$$\begin{aligned} f_{\text{on } a} &= - \sum_{\Delta: a \in \Delta} \frac{d}{d\mathbf{r}_a} \sum_{b \in \Delta} \left(\mathbf{r}_b - \frac{1}{n} \sum_{c \in \Delta} \mathbf{r}_c \right)^2 \\ &= \sum_{\Delta: a \in \Delta} \sum_{b \in \Delta} \left(2\mathbf{r}_a \delta_{ab} - \frac{2}{n} \sum_{c \in \Delta} (\mathbf{r}_c \delta_{ab} + \mathbf{r}_b \delta_{ac}) + \frac{1}{n^2} \sum_{c \in \Delta} \sum_{d \in \Delta} (\delta_{ac} \mathbf{r}_d + \delta_{ad} \mathbf{r}_c) \right) \\ &= -2(\mathbf{r}_a - \mathbf{r}_{\Delta}) \end{aligned}$$

This process was overkill, since we could have reasonably assumed that \mathbf{r}_{Δ} would be at the vertices' center of mass and that we'd effectively get springs from \mathbf{r}_{Δ} to each vertex. This is thanks to linearity of the collar springs. However, assuming that the collars have a positive equilibrium length r_0 makes it necessary to go through the above procedure.

If instead the line energy is

$$\mathcal{E}_{ab} = \int_0^1 (|\mathbf{r}_a t + (1-t)\mathbf{r}_b - \mathbf{r}_{\Delta}| - r_0)^2 dt,$$

then the cell position \mathbf{r}_{Δ} is the solution to

$$\begin{aligned} 0 &= -2 \sum_{b \in \Delta} \mathbf{r}_b + 6\mathbf{r}_{\Delta} - 2r_0 \frac{d}{d\mathbf{r}_{\Delta}} \sum_{(b,c) \text{ edge in } \Delta} \int_0^1 |\mathbf{r}_b t - (1-t)\mathbf{r}_c - \mathbf{r}_{\Delta}| dt \\ 0 &= -2 \sum_{b \in \Delta} \mathbf{r}_b + 6\mathbf{r}_{\Delta} - 2r_0 \sum_{(b,c)} \int_0^1 \frac{\mathbf{r}_{\Delta} - \mathbf{r}_c - t(\mathbf{r}_b - \mathbf{r}_c)}{|\mathbf{r}_b t - (1-t)\mathbf{r}_c - \mathbf{r}_{\Delta}|} dt. \end{aligned}$$

We can actually evaluate the integral above, but I found that it gives a transcendental equation for \mathbf{r}_{Δ} and decided it wasn't pursuing further on paper. Nonzero equilibrium length springs is better pursued numerically. Alternatively, we simply define springs from \mathbf{r}_{Δ} to each dual graph vertex rather than making the collars consist of continuous springs.

Bending

One way to define a bending energy is to give each cell a vector that corresponds to the midline pointing out from the center of the cell, which I have implicitly drawn in the figures of individuals flexas. From there, we could reasonably define a bending energy from the interactions between two interacting flexas by the angle between their corresponding “normal” vectors weighted by the length of their interface.

Defining an individual vector is made complicated by the fact that the vertices along the cycles corresponding to each flexa are not necessarily coplanar, provided that a given cell is interacting with more than three other cells. One option, although I have not developed it, is to find the plane whose summed mean squared distances to each vertex for a cell is minimised. It would possibly be more accurate to again treat the edges as lines and minimise the integrated distance from the normal plane to the edges. Either way, the energy dictated by the angle between adjacent normal vectors will need to be summed over all pairs of neighboring cells, namely all edges in the graph where edges correspond to cell neighbors (not collar interfaces).

3.3.3 Surface formed by cell bodies

The graph of cell bodies and neighbor edges makes it easy to work with springs, but it is less clear how to define a bending energy. The math for springs is identical to previously, so let’s just think about how to define bending energy.

needs more work

3.4 Including both cells and collar boundaries**3.4.1 Initial sheet**

Let’s call the graph of cells with cell-cell neighbor relations as edges G , and the dual graph of collar boundaries G^* . For setting up the network topology, we proceed by defining G to lie in the xy -plane with a set of cell coordinates $\{\mathbf{r}_c\}_{c \in C}$ for the set of cells C and using Voronoi tessellation to build G^* . This is nice because it generalises beyond regular lattices. The curvature will be built in later when minimising the sheet energy.

We can build a super graph \mathfrak{G} which has both the cell positions and collar boundaries, as well as edges from each cell c to the boundary vertices b in the cell’s set of collar boundary

1 vertices $B_c \in V^*$. That is, \mathfrak{G} has the cell-cell neighbor edges E between cell vertices C , collar
 2 vertices V^* , and edges $\{\{(c, b)\}_{b \in B_c}\}_{c \in C}$.

3 Since Voronoi regions for cells that aren't completely surrounded by other cells (which I
 4 will call *boundary cells*) extend out to infinity, we need to create a new vertex at each infinite
 5 boundary to make a finite collar boundary. (Figure 3.2)

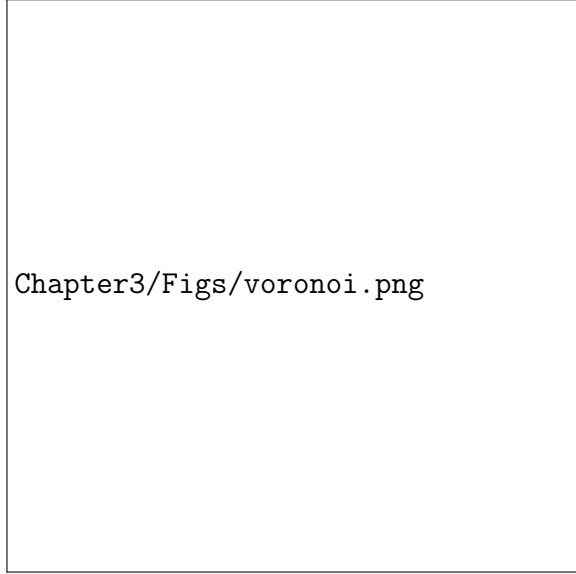


Fig. 3.2 Voronoi tessellation of initial cell placement. Cell bodies shown in blue points, collar boundaries shown in black lines with collar boundary end points shown in orange. Notably, the regions corresponding to boundary cells extend out to infinity. We need to add all boundary collar vertices along the infinite dashed lines.

6 Why do boundary collar vertices matter?

7 Does it matter that boundary cells have collar nodes at the boundary? We can answer this
 8 analytically. For cells a, c and mutual interior collar boundary vertex b , suppose the physically
 9 finite collar boundary ends at point \mathbf{r} . We want to know how the angle between the planes
 10 $\mathbf{r}_a, \mathbf{r}_b, \mathbf{r}$ and $\mathbf{r}_c, \mathbf{r}_b, \mathbf{r}$ changes as \mathbf{r} changes.

11 For now let's say that the collar length is fixed as ℓ , so the range of motion of \mathbf{r} is
 12 constrained. We can simplify our problem by reparameterising our coordinates such that $\mathbf{r}_a =$
 13 $(-1, 0, 0)$, $\mathbf{r}_b = (0, r, 0)$, and $\mathbf{r}_c = (1, 0, 0)$, where $r = \sqrt{\ell^2 - 1}$. Note that ℓ is a dimensionless
 14 ratio of the collar length to cell-cell distance here.¹ It is easy to show that the solution set
 15 for allowable values of \mathbf{r} is given by solutions satisfying $r^2 = y^2 + z^2$, $x = 0$. Equivalently,

¹Later we will use ℓ as the only length scale in the problem when we're solving the sheet shape by minimising energy.

3.4 Including both cells and collar boundaries

25

the possible vectors $\mathbf{r}(\theta)$ are $(0, r \cos \theta, r \sin \theta)$. So let's find the normal vectors between the two collar-cell-collar surfaces to see if the plane-plane angle changes with θ .

We have the normals are

$$\begin{aligned}\hat{\mathbf{n}}_1 &= (\mathbf{r} - \mathbf{r}_a) \times (\mathbf{r}_b - \mathbf{r}_a) \\ &= \frac{(-r^2 \sin \theta, r \sin \theta, r - r \cos \theta)}{r^4 \sin^2 \theta + 2r^2(1 - \cos \theta)} \\ \hat{\mathbf{n}}_2 &= (\mathbf{r}_b - \mathbf{r}_c) \times (\mathbf{r} - \mathbf{r}_c) \\ &= \frac{(r^2 \sin \theta, r \sin \theta, r \cos \theta - r)}{r^4 \sin^2 \theta + 2r^2(1 - \cos \theta)}.\end{aligned}$$

Their angle is given by (after simplifying)

$$\hat{\mathbf{n}}_1 \cdot \hat{\mathbf{n}}_2 = 1 - \frac{2}{1 + \frac{1}{2r^2} (1 + \tan^2 \frac{\theta}{2})}.$$

The point is that the plane-plane angle changes with θ ! So the boundary collar nodes really have an effect on the sheet energy, and we need to include them. This is an important result too since (as Lloyd always reminds me) the boundary conditions affect the whole shape of the sheet. So one way to conceivably move the sheet is by updating the boundary collar nodes then working inward to update the whole sheet shape.

Regardless, this tells us that we need to add our own boundary collar nodes to our simulation, since they aren't provided by the Voronoi tessellation.

Adding boundary collar vertices

The coordinate system for each cell-cell neighbor pair we developed in the previous section is useful for creating our own new boundary collar vertices. For two boundary cell positions $\mathbf{r}_{c_1}, \mathbf{r}_{c_2}$, we can take the orthogonal component of $\mathbf{r}_b - \mathbf{r}_{c_1}$ (where b is the existing collar boundary node between c_1, c_2) with respect to $\mathbf{r}_{c_1} - \mathbf{r}_{c_2}$. Adding this orthogonal component to the cells' center of mass $(\mathbf{r}_{c_1} + \mathbf{r}_{c_2})/2$ (which is on the Voronoi boundary) will give a new position equidistant from the two cells, where the cell-collar lengths is the same as that to the existing collar boundary vertex.

The resulting cell sheet and collar boundary surface is shown in Figure 3.3. Notice in particular that every cell on the boundary has two collar nodes between it and its neighboring cells on the boundary. This whole graph \mathcal{G} is shown projected onto the xy -plane, but the collar interactions are all offset in z relative to the cells.

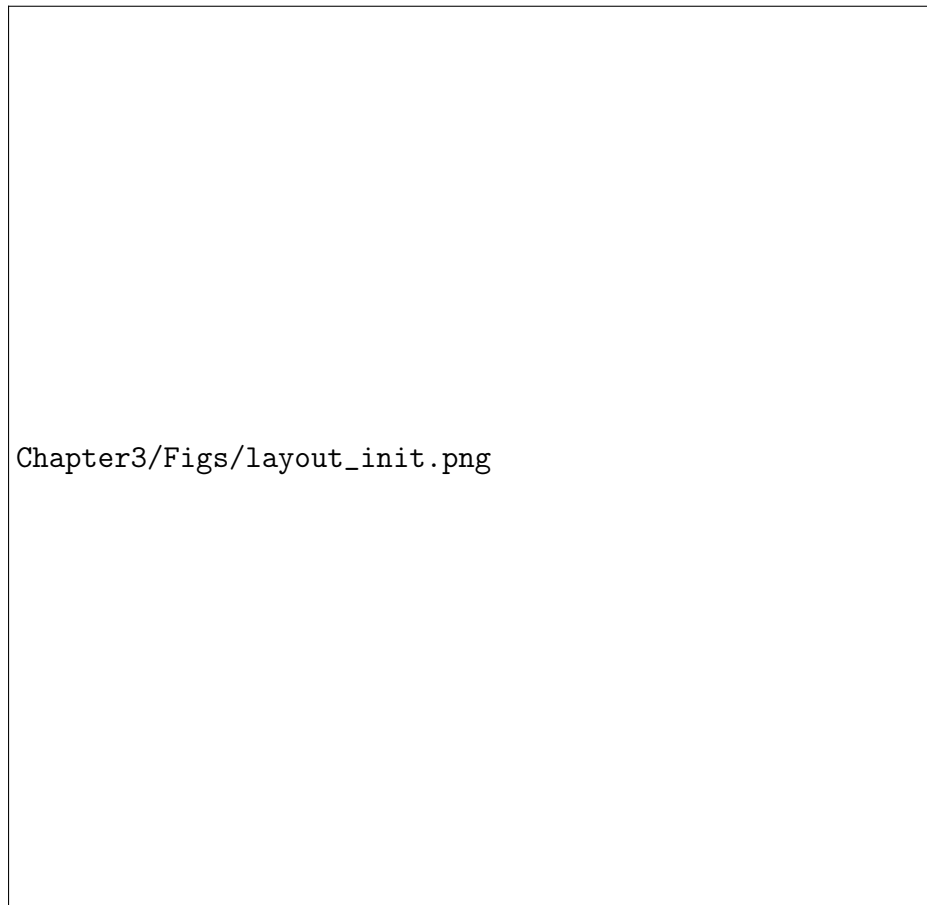


Fig. 3.3 Initial layout for the flexa sheet. Cell bodies are shown in large purple points and collar boundary vertices are shown in small yellow points. Black edges connect cells to collar boundary vertices, and orange edges show cell-cell neighbor relations (though these orange edges are not physically present). The physical interactions are mediated through the black edges.

3.4.2 Bending energies

Collar length

For now, we are going to take the collar lengths to be fixed at their initial lengths. Since we're using a regular lattice for now, we can define this as ℓ to be the only length in our problem. (Cell-cell distance will change when we minimise the energy.)

Later, it would be nice to add a collar length energy term $(|\mathbf{r}_c - \mathbf{r}_{b_c}| - r_0)^2$ term that makes the cell-collar lengths flexible.

Cell-collar angle ϕ energy

The paper we're basing our work on defines the collar angle ϕ relative to the direction of the cell body \hat{n}_c for cell c . Immediately, we run into a problem, which is that \hat{n} is not clearly defined when the cell is interacting with several other cells. When that happens, the cell's collar does not necessarily form its boundaries in a plane.

Defining the cell normal vector \hat{n}_c We can define the cell's vector \hat{n}_c for a cell c by taking the average vector from \mathbf{r}_c to \mathbf{r}_b for all collar boundary nodes $b \in B_c$. However, we run into a problem for boundary cells, which is that this normal vector then points inward towards the sheet because we didn't define collar boundary nodes that don't connect to other cells. In the language of Figure 3.3, the boundary cells have less than a symmetric set of 6 collar boundary nodes.

This doesn't agree with our intuition, since the entire sheet is flat. So we expect the cells at the boundaries to have vectors \hat{n}_c pointing directly in $+\hat{z}$ (as the collars are above the cell sheet in z). Instead, we can define \hat{n}_c by taking a plane approximation to the collar boundary position vectors $\{\mathbf{r}_b\}_{b \in B_c}$. This plane defines a normal vector.

If we approximate $\hat{z}_b = (x_b, y_b) \cdot (\beta_1, \beta_2) + \beta_0$ and minimize the sum of squared residuals $\sum_{b \in B_c} (\hat{z}_b - z_b)^2$ with respect to $\beta_0, \beta_1, \beta_2$,² then the normal vector of the plane approximation is $(\beta_1, \beta_2, -1)$ up to normalisation and multiplication by -1 .

We need to orient the cell's vector \hat{n}_c so that it points in the direction from the cell to the collar. Fortunately, we could use the average cell-to-collar vector that we discussed before to do this alignment.

²We do this with ordinary least squares, which is why I use the notation \hat{z}_b and β .

What is the best normal vector for a cell? Suppose a cell is at position \mathbf{r}_c with collar vertices at \mathbf{r}_b for $b \in B_c$. We can ask how the cell orients itself to minimise its collar energy in ϕ . The energy of the cell \mathcal{E}_c is given by

$$\mathcal{E}_c = \sum_{b \in B_c} \left[\arccos \left(\frac{\mathbf{r}_b - \mathbf{r}_c}{|\mathbf{r}_b - \mathbf{r}_c|} \cdot \hat{\mathbf{n}}_c \right) - \phi_0 \right]^2.$$

We can ask what normal vector minimises \mathcal{E}_c by setting the gradient of \mathcal{E}_c with respect to $\hat{\mathbf{n}}_c$ to zero. But the length of $\hat{\mathbf{n}}_c$ is fixed at one, so we solve

$$0 = \frac{\partial \left[\mathcal{E}_c + \lambda \left(|\hat{\mathbf{n}}_c|^2 - 1 \right) \right]}{\partial \hat{\mathbf{n}}_c}$$

subject to $|\hat{\mathbf{n}}_c|^2 = 1$. I found that

$$\lambda \hat{\mathbf{n}}_c = 2 \sum_{b \in B_c} \left[\arccos \left(\frac{\mathbf{r}_b - \mathbf{r}_c}{|\mathbf{r}_b - \mathbf{r}_c|} \cdot \hat{\mathbf{n}}_c \right) - \phi_0 \right] \frac{-1}{\sqrt{1 - \left(\frac{\mathbf{r}_b - \mathbf{r}_c}{|\mathbf{r}_b - \mathbf{r}_c|} \cdot \hat{\mathbf{n}}_c \right)^2}} \frac{\mathbf{r}_b - \mathbf{r}_c}{|\mathbf{r}_b - \mathbf{r}_c|}$$

$$\lambda = 2 \left| \sum_{b \in B_c} \left[\arccos \left(\frac{\mathbf{r}_b - \mathbf{r}_c}{|\mathbf{r}_b - \mathbf{r}_c|} \cdot \hat{\mathbf{n}}_c \right) - \phi_0 \right] \frac{1}{\sqrt{1 - \left(\frac{\mathbf{r}_b - \mathbf{r}_c}{|\mathbf{r}_b - \mathbf{r}_c|} \cdot \hat{\mathbf{n}}_c \right)^2}} \frac{\mathbf{r}_b - \mathbf{r}_c}{|\mathbf{r}_b - \mathbf{r}_c|} \right|.$$

Then

$$\hat{\mathbf{n}}_c = \frac{\sum_{b \in B_c} \left[\arccos \left(\frac{\mathbf{r}_b - \mathbf{r}_c}{|\mathbf{r}_b - \mathbf{r}_c|} \cdot \hat{\mathbf{n}}_c \right) - \phi_0 \right] \frac{-1}{\sqrt{1 - \left(\frac{\mathbf{r}_b - \mathbf{r}_c}{|\mathbf{r}_b - \mathbf{r}_c|} \cdot \hat{\mathbf{n}}_c \right)^2}} \frac{\mathbf{r}_b - \mathbf{r}_c}{|\mathbf{r}_b - \mathbf{r}_c|}}{\left| \sum_{b' \in B_c} \left[\arccos \left(\frac{\mathbf{r}_{b'} - \mathbf{r}_c}{|\mathbf{r}_{b'} - \mathbf{r}_c|} \cdot \hat{\mathbf{n}}_c \right) - \phi_0 \right] \frac{1}{\sqrt{1 - \left(\frac{\mathbf{r}_{b'} - \mathbf{r}_c}{|\mathbf{r}_{b'} - \mathbf{r}_c|} \cdot \hat{\mathbf{n}}_c \right)^2}} \frac{\mathbf{r}_{b'} - \mathbf{r}_c}{|\mathbf{r}_{b'} - \mathbf{r}_c|} \right|}$$

Calculating collar angle ϕ Once we have a cell normal vector \hat{n}_c for each cell c , it is easy to calculate the collar angles ϕ_{cb} to each collar boundary vertex $b \in B_c$. Now, indexing over all cell-collar edges in \mathfrak{G} (black edges in Figure 3.3), we write the ϕ energy

$$\mathcal{E}_\phi = \sum_{c \in C} \sum_{b \in B_c} (\phi_{cb} - \phi_0)^2 = \sum_{(c,b) \in \{\text{cell-collar edges } (c,b)\}} (\phi_{cb} - \phi_0)^2.$$

When ϕ_0 is equal to the initial angle between $\hat{\mathbf{z}}$ (which is the initial \hat{n}_c for each cell c) and each cell-collar vector $\mathbf{r}_b - \mathbf{r}_c$ (which is well-defined because we're using a regular lattice to start), we get that $\mathcal{E}_\phi = 0$ numerically. This confirms that our code is calculating the energy right. Of course this energy will be nonzero when ϕ_0 differs from the initial angle.

Cell-cell junction angle ψ energy

We suppose that there is also an energy \mathcal{E}_ψ based on the angle ψ that two cells make at their mutual collar boundary. We can calculate this as we did previously, where we found that the length of collar boundary (equivalently, the angle θ between the two collar nodes and each cell) affects the cell-collar-cell angle. Let's say there's an equilibrium angle ψ_0 between two cell collars.

For cells c_1, c_2 and mutual collar boundary vertices b, b' , we define $\hat{\mathbf{n}}_1$ and $\hat{\mathbf{n}}_2$ as the normal vectors to planes defined by $\mathbf{r}_{c_1}, \mathbf{r}_b, \mathbf{r}_{b'}$ and $\mathbf{r}_{c_2}, \mathbf{r}_b, \mathbf{r}_{b'}$. The angle between these planes is given as $\hat{\mathbf{n}}_1 \cdot \hat{\mathbf{n}}_2$, and the acute angle on the interior of the hinge is $\pi - \arccos(\hat{\mathbf{n}}_1 \cdot \hat{\mathbf{n}}_2)$.

Let's assume that the angle ψ is shared evenly between the two cells, so that the cell c_1 contribution to \mathcal{E}_ψ is $(\psi_{c_1, c_2}/2 - \psi_0/2)^2$ for cell-cell neighbor relation (c_1, c_2) . Likewise for c_2 . Then \mathcal{E}_ψ indexes over the cell-cell neighbor relations in edge set E :

$$\mathcal{E}_\psi = \sum_{(c_1, c_2) \in E} (\psi_{c_1, c_2}/2 - \psi_0/2)^2.$$

Flat sheet as a solution

Notice that we have a pair (ϕ_0, ψ_0) that gives $\mathcal{E} = \mathcal{E}_\phi + \mathcal{E}_\psi = 0$. Since the ϕ and ψ energies are nonnegative, the flat sheet is a stable minimum.

3.4.3 Minimising sheet energy

We now have an energy $\mathcal{E}\{\mathbf{r}_v\}_{v \in \mathcal{G}} = \mathcal{E}_\phi + \mathcal{E}_\psi$ which is parameterised over the cell and collar boundary vertex positions. Notably, we treat the topology of the network as fixed, so the indices of the summations for \mathcal{E}_ϕ and \mathcal{E}_ψ are unchanged even as we minimise energy.

Constant collar length constraint

For now, we are numerically constraining the cell-collar lengths at ℓ , their initial lengths (which are constant for all cells). If we want to use the generalisability of our model to use an random initial cell distribution and generate the irregular boundaries with Voronoi tessellation, we will have to relax this condition and add a collar length spring energy to \mathcal{E} . The constant collar length constraint only applies to sheets generated by regular lattices when laid flat on a plane.

The constraint is defined by a vector function $f((c, b)) = |\mathbf{r}_c - \mathbf{r}_b| - \ell = 0$ for all cell-collar edges (c, b) . If n_{collars} is the number of cell-collar edges in $\{\text{cell-collar edges } (c, b)\}$, then f defines a n_{collars} -vector function.

My optimisation routine requires that we calculate a Jacobian matrix for the vector constraint function. This gets ugly if we use f as written above, but it is fortunately equivalent to set the constraint $f'((c, b)) = |\mathbf{r}_c - \mathbf{r}_b|^2 - \ell^2 = 0$. It is an interesting problem to take the gradient of \mathbf{f}' with respect to all of the coordinates, but I won't include it here. It's implemented in my code.

3.4.4 Numerical optimisation routine

Finally, we numerically optimise. I changed ϕ_0 to be defined relative to the initial value of ϕ , and likewise for ψ . If we make ϕ_0 smaller and ψ_0 larger, we expect the cell collars to contract and for cell-cell distances to lengthen. In other words, we expect the sheet to curve upward, so that the cells on the edges go in the direction that the collars are.

The numerical optimisation problem gives a clean sensible solution, which is shown projected onto the xy -plane in Figure 3.4. We can tell that the sheet is curved just looking at this alone, which is a massive relief and confirmation of what we expect.

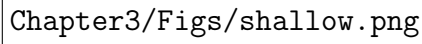
The solution in Figure 3.4 is for $\phi_0 = 0.99\phi_{\text{init}}$ and $\psi_0 = 1.03\psi_{\text{init}}$, where ϕ_{init} and ψ_{init} are the initial angles in the flat sheet state. We could now bask in the glory of our solution and look at it in 3d (Figure 3.5a).

The resulting structure is really pretty sensitive to small changes in ϕ_0, ψ_0 . Figure 3.5b shows the structure that comes out of $\phi_0 = 0.9\phi_{\text{init}}, \psi_0 = 1.15\psi_{\text{init}}$.



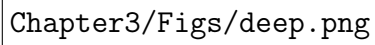
Chapter3/Figs/layout_curved.png

Fig. 3.4 Figure in the same style of Figure 3.3 showing the cell sheet projected onto the xy -plane after minimising energy.



Chapter3/Figs/shallow.png

(a)



Chapter3/Figs/deep.png

(b) 3d projections of the curved sheet formed by $\phi_0 = 0.9\phi_{\text{init}}$, $\psi_0 = 1.15\psi_{\text{init}}$.

Fig. 3.5 Cell sheet geometry from the hexagonal lattice in Figure 3.3 and parameters (3.5a) $\phi_0 = 0.99\phi_{\text{init}}$, $\psi_0 = 1.03\psi_{\text{init}}$, $\ell_0 = \ell_{\text{init}} = 1.52$, (3.5b) $\phi_0 = 0.9\phi_{\text{init}}$, $\psi_0 = 1.15\psi_{\text{init}}$, $\ell_0 = \ell_{\text{init}} = 1.52$.

3.4.5 Topology

In section 3.4.2, I mentioned that the flat sheet is a stable minimum. But it is here because the lattice is regular. A single pentagon in a hexagonal lattice (like a football (soccer) ball, thanks Lloyd) will make it so no ϕ_0 and ψ_0 will make every cell make the other cells flat.

What I think is interesting about this is the connection between graph topology and surface geometry. I think, in a continuous sense, graph topology affects Gaussian curvature through the energy function.

Adding noise to initial cell positions in Figure 3.3

We expect the initial lattice in Figure 3.3 to produce a sheet with 6-fold symmetry. Since the graph of connections is produced by a Voronoi tessellation, small changes to initial boundary cell positions can change the graph topology for boundary cells.

When adding noise to the initial cell positions, the change in topology at some boundary nodes results in substantial effects felt over the sheet. Figure 3.6 shows the effect of different topology at the boundary.

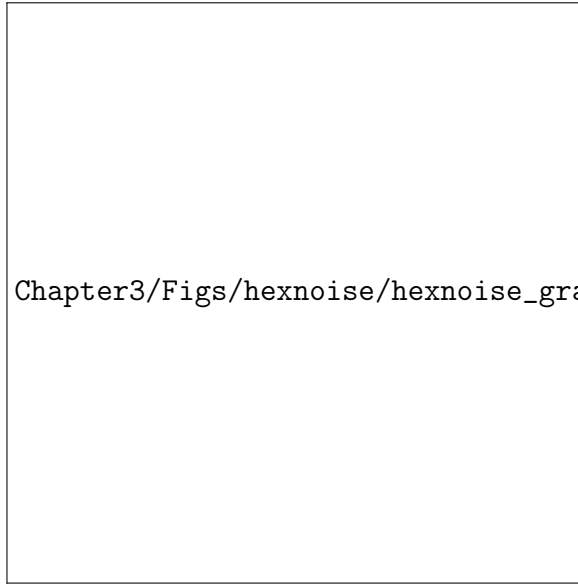
Interior cell topology

We can also add or merge nodes in a regular lattice (Figure 3.3) to introduce nodes with irregular degree. There are more complex ways of making different graph topologies (like Lloyd's initial icosphere) but I don't have curved initial conditions or more complicated lattices implemented yet.

Figure 3.7 shows a sheet with cell of degree 7 (7 bordering cells) and 3.8 shows a sheet with two neighboring cells of degree 5.

3.4.6 Larger cell sheets

If inverting a sheet of cells involves flattening it out at the edges, then a small sheet will be able to do this easier than a large one. This is because the cells on the outside have to stretch their collars less if the sheet is smaller when they flatten out.



(a) Initial lattice drawn as in Figure 3.3.

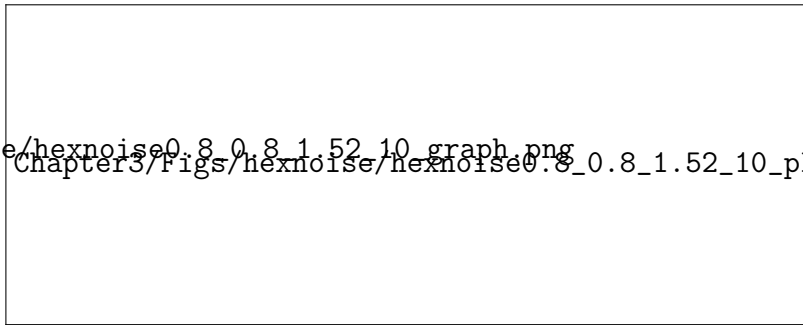
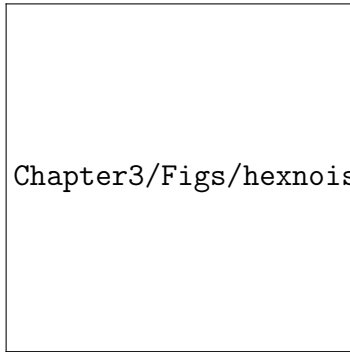
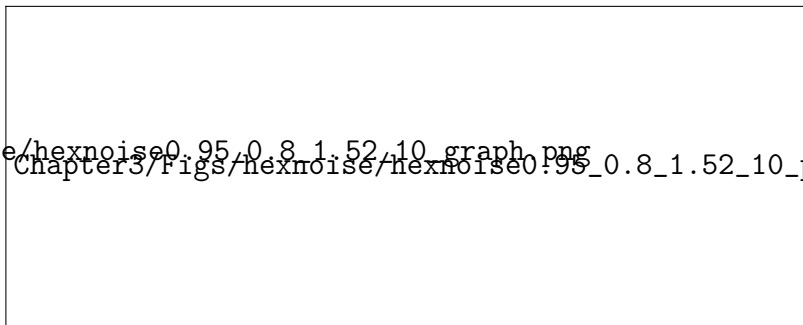
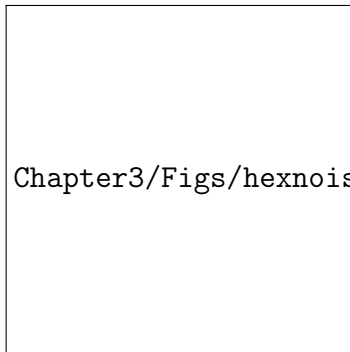
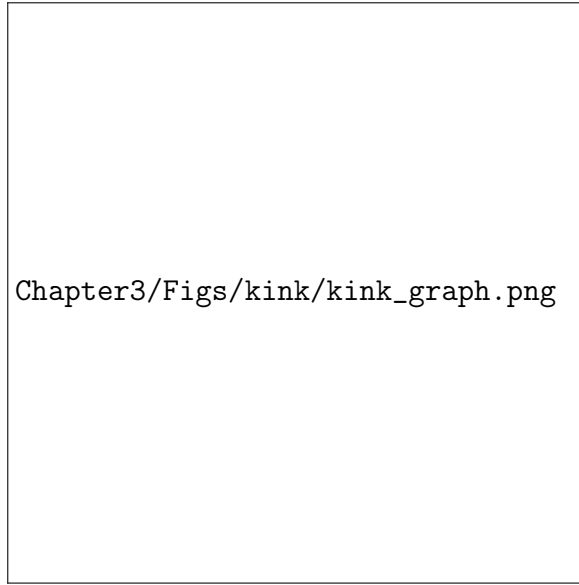
(b) Sheet shape when $\phi_0 = 0.8$, $\psi_0 = 0.8$, $\ell_0 = 1.52$.(c) Sheet shape when $\phi_0 = 0.95$, $\psi_0 = 0.8$, $\ell_0 = 1.52$.

Fig. 3.6 Cell sheet geometry with noise added to the initial lattice. The graph topology is affected at the sheet boundary (subfigure 3.6a) from the Voronoi tessellation. This minor change has substantial effects on the sheet geometry (subfigures 3.6b, 3.6c).



(a) Initial lattice drawn as in Figure 3.3.

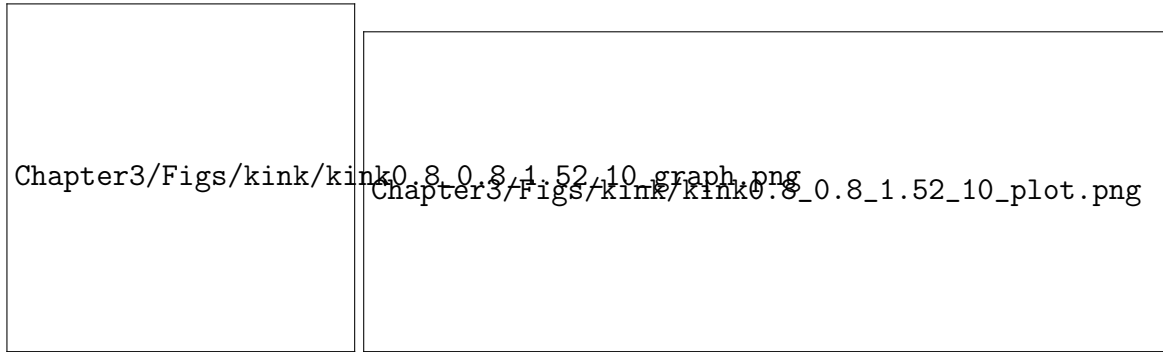
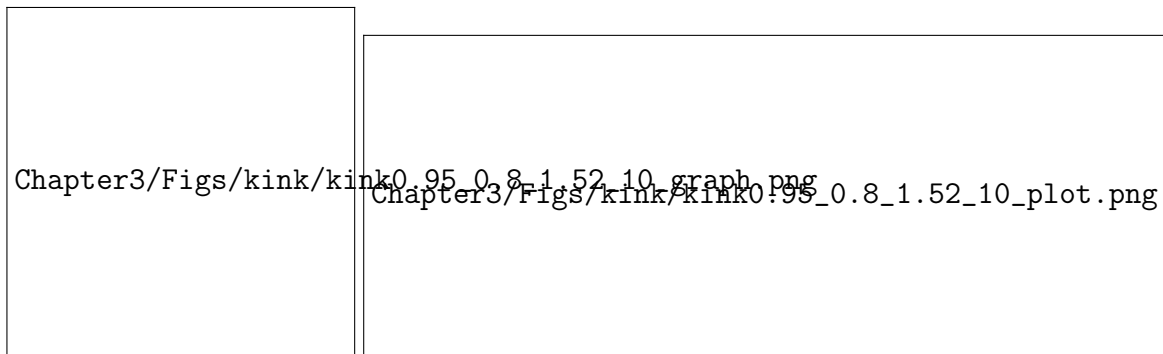
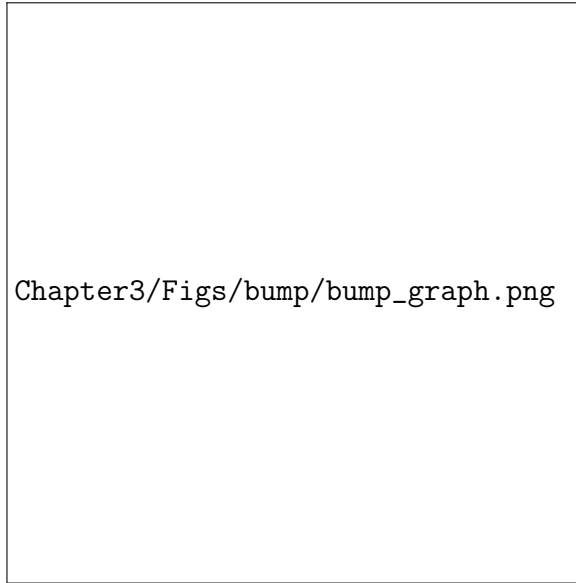
(b) Sheet shape when $\phi_0 = 0.8$, $\psi_0 = 0.8$, $\ell_0 = 1.52$.(c) Sheet shape when $\phi_0 = 0.95$, $\psi_0 = 0.8$, $\ell_0 = 1.52$.

Fig. 3.7 Cell sheet geometry with a node of degree 7. The graph topology is affected in the sheet interior (subfigure 3.7a). This minor change has substantial effects on the sheet geometry (subfigures 3.7b, 3.7c).



(a) Initial lattice drawn as in Figure 3.3.

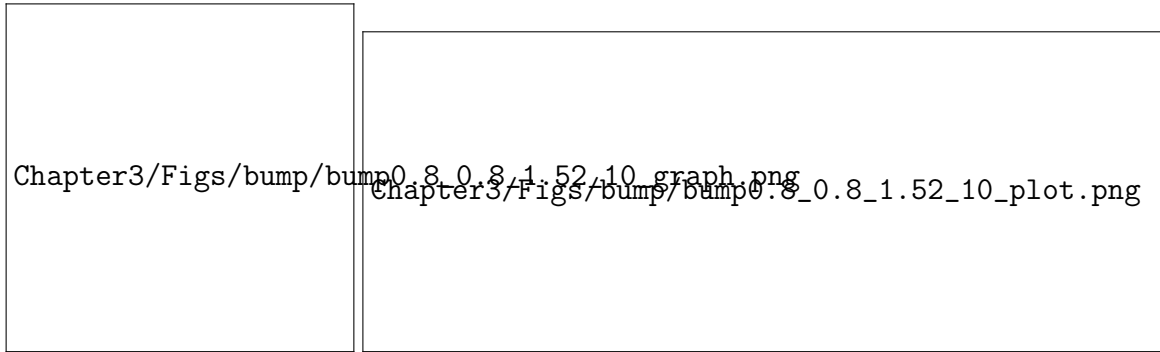
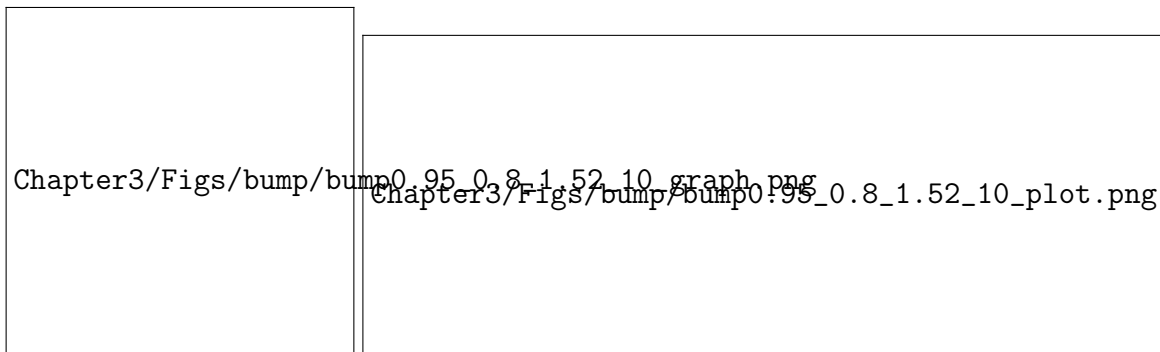
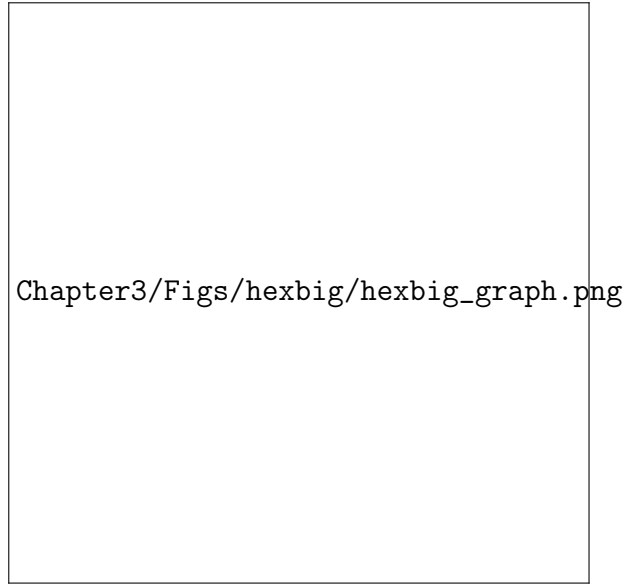
(b) Sheet shape when $\phi_0 = 0.8$, $\psi_0 = 0.8$, $\ell_0 = 1.52$.(c) Sheet shape when $\phi_0 = 0.95$, $\psi_0 = 0.8$, $\ell_0 = 1.52$.

Fig. 3.8 Cell sheet geometry with a node of degree 7. The graph topology is affected in the sheet interior (subfigure 3.8a). This minor change has substantial effects on the sheet geometry (subfigures 3.8b, 3.8c).



(a) Initial lattice drawn as in Figure 3.3.

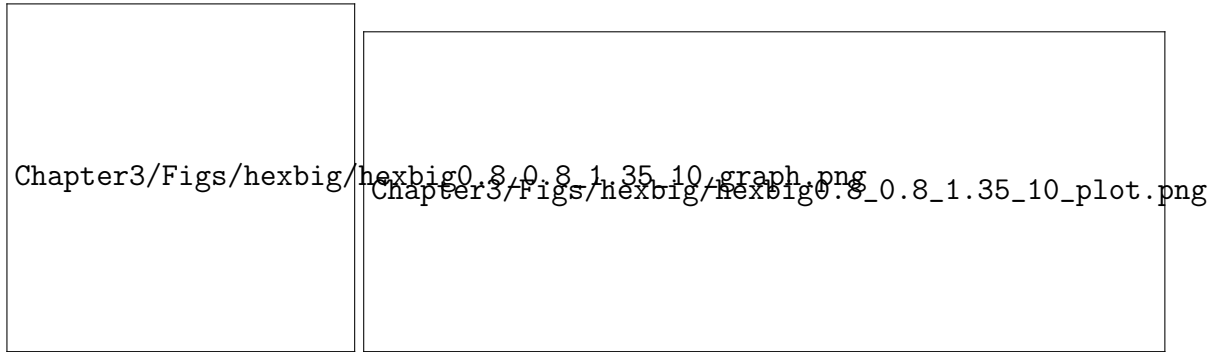
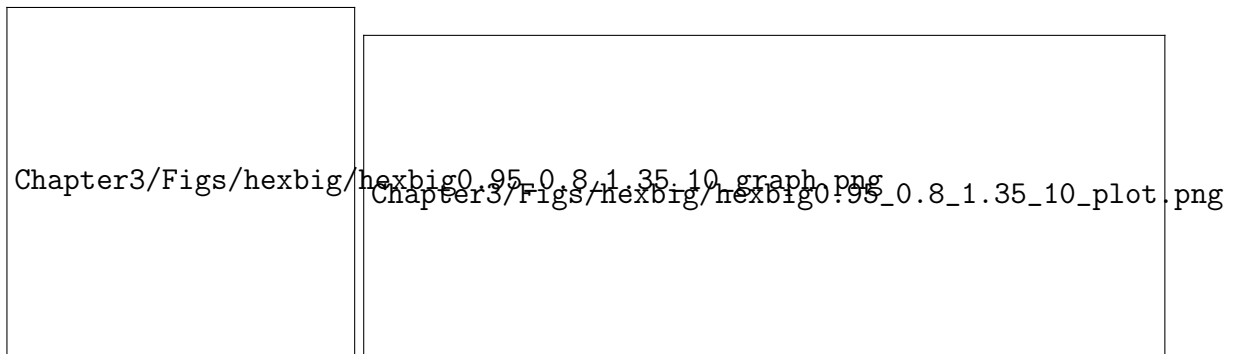
(b) Sheet shape when $\phi_0 = 0.8$, $\psi_0 = 0.8$, $\ell_0 = 1.52$.(c) Sheet shape when $\phi_0 = 0.95$, $\psi_0 = 0.8$, $\ell_0 = 1.52$.

Fig. 3.9 Cell sheet geometry with a node of degree 7. The graph topology is affected in the sheet interior (subfigure 3.9a). This minor change has substantial effects on the sheet geometry (subfigures 3.9b, 3.9c).

3.5 Varying the energy

$$\vec{F}_\gamma = \frac{\partial E}{\partial \vec{r}_\gamma} = 2 \sum_{(\alpha, \rho)} (\phi_{(\alpha, \rho)} - \phi_0) \frac{\partial \phi_{(\alpha, \rho)}}{\partial \vec{r}_\gamma} + 2 \sum_{(\alpha, \beta: \sigma, \rho)} (\psi(\hat{\mathbf{n}}_{\sigma\alpha\rho}, \hat{\mathbf{n}}_{\sigma\beta\rho}) - \psi_0) \frac{\partial \psi_{(\alpha, \beta: \sigma, \rho)}}{\partial \vec{r}_\gamma}$$

$$\frac{\partial \phi_{(\alpha, \rho)}}{\partial r_{\gamma i}} = \frac{-1}{\sqrt{1 - (\hat{\mathbf{n}}_\alpha \cdot (\hat{\alpha}\rho))^2}} \left(\frac{\partial \hat{\mathbf{n}}_{\alpha j}}{\partial r_{\gamma i}} (\hat{\alpha}\rho)_j + \frac{\partial (\hat{\alpha}\rho)_j}{\partial r_{\gamma i}} \hat{\mathbf{n}}_{\alpha j} \right)$$

$$\frac{\partial (\hat{\alpha}\rho)_j}{\partial r_{\gamma i}} = \frac{(\delta_{\gamma\rho} - \delta_{\gamma\alpha})}{|r_\rho - r_\alpha|} (\delta_{ij} + (\hat{\alpha}\rho)_i (\hat{\alpha}\rho)_j)$$

$$\frac{\partial \hat{\mathbf{n}}_{\alpha j}}{\partial r_{\gamma i}} = \frac{\mathbb{I}_{\gamma \in \text{collars}(\alpha)} - n \delta_{\gamma\alpha}}{|\sum_{(\alpha, \rho)} (r_\rho - r_\alpha)|} (\delta_{ij} - \hat{\mathbf{n}}_{\alpha i} \hat{\mathbf{n}}_{\alpha j})$$

$$\frac{\partial \psi_{(\alpha, \beta: \sigma, \rho)}}{\partial r_{\gamma i}} = \frac{-1}{\sqrt{1 - (\hat{\mathbf{n}}_{\rho\alpha\sigma} \cdot \hat{\mathbf{n}}_{\rho\beta\sigma})^2}} \left(\frac{\partial \hat{\mathbf{n}}_{\rho\alpha\sigma j}}{\partial r_{\gamma i}} \hat{\mathbf{n}}_{\rho\beta\sigma j} + \frac{\partial \hat{\mathbf{n}}_{\rho\beta\sigma j}}{\partial r_{\gamma i}} \hat{\mathbf{n}}_{\rho\alpha\sigma j} \right)$$

$$\frac{\partial \hat{\mathbf{n}}_{\rho\alpha\sigma j}}{\partial r_{\gamma i}} = \text{too big see notes}$$

Chapter 4

Discussion

4.1 section

Think about why *C. flexa* has the behavior that it does. Given how other choanoflagellates like *S. rosetta* get their morphology by division [5, 7], it could be that *C. flexa* forms by division and has evolved its contractile ring to take advantage of that. This would make sense from the perspective that choanoflagellate cells aligned and lined up next to each other drive the strongest flows (though still not stronger than they could individually) Kirkegaard and Goldstein [6]. This paper also found that being farther from a wall increases flux. This is interesting considering that the feeding state of *C. flexa* was observed to be so ineffective at swimming that it sank and remained in place. However this was on a slide and in the absense of external flows Brunet et al. [3].

When thinking about *C. flexa* in the context of multicellularity, we should not overlook the simplicity by which it achieves large-scale geometric changes. While we can develop increasingly complex models by introducing collar filament bending, tension and stress at the collar filaments' bases, or the effects of the contractile ring, my work demonstrates that a coarse description of individual cells is sufficient to explain the behavior that we observe in colonies. Compare this with *Volvox*, which uses connections and communication between cells to control its inversion. One might imagine that the complexity of a molecular pathway for a single cell to exhibit phototaxis or regulate feeding/swimming efficiency could easily exceed the ring contraction as currently understood in *C. flexa* [3].

ak2351: cite Volvox inversion papers, cite papers on phototaxis or swimming signalling pathways

References

- [1] Alegado, R. A., Brown, L. W., Cao, S., Dermenjian, R. K., Zuzow, R., Fairclough, S. R., Clardy, J., and King, N. (2012). A bacterial sulfonolipid triggers multicellular development in the closest living relatives of animals. *elife*, 1. 2 3 4
- [2] Asadzadeh, S. S., Larsen, P. S., Riisgård, H. U., and Walther, J. H. (2019). Hydrodynamics of the leucon sponge pump. *Journal of the Royal Society Interface*, 16(150):20180630. 5 6
- [3] Brunet, T., Larson, B. T., Linden, T. A., Vermeij, M. J., McDonald, K., and King, N. (2019). Light-regulated collective contractility in a multicellular choanoflagellate. *Science*, 366(6463):326–334. 7 8 9
- [4] Carr, M., Leadbeater, B. S., Hassan, R., Nelson, M., and Baldauf, S. L. (2008). Molecular phylogeny of choanoflagellates, the sister group to metazoa. *Proceedings of the National Academy of Sciences*, 105(43):16641–16646. 10 11 12
- [5] Fairclough, S. R., Dayel, M. J., and King, N. (2010). Multicellular development in a choanoflagellate. *Current Biology*, 20(20):R875–R876. 13 14
- [6] Kirkegaard, J. B. and Goldstein, R. E. (2016). Filter-feeding, near-field flows, and the morphologies of colonial choanoflagellates. *Physical Review E*, 94(5):052401. 15 16
- [7] Larson, B. T., Ruiz-Herrero, T., Lee, S., Kumar, S., Mahadevan, L., and King, N. (2020). Biophysical principles of choanoflagellate self-organization. *Proceedings of the National Academy of Sciences*, 117(3):1303–1311. 17 18 19
- [8] Leadbeater, B. S. C. (2008). Choanoflagellate evolution: the morphological perspective. *Protistology*, 5:256–267. 20 21
- [9] Mah, J. L., Christensen-Dalsgaard, K. K., and Leys, S. P. (2014). Choanoflagellate and choanocyte collar-flagellar systems and the assumption of homology. *Evolution & development*, 16(1):25–37. 22 23 24
- [10] Michelin, S. and Lauga, E. (2011). Optimal feeding is optimal swimming for all péclet numbers. *Physics of Fluids*, 23(10):101901. 25 26
- [11] Powers, T. R. (2010). Dynamics of filaments and membranes in a viscous fluid. *Reviews of Modern Physics*, 82(2):1607. 27 28

